

Banner appropriate to article type will appear here in typeset article

Phenomenology of decaying turbulence beneath surface waves

Gregory L. Wagner¹† and Navid C. Constantinou^{2,3}

¹Massachusetts Institute of Technology, Cambridge, MA, USA

²University of Melbourne, Parkville, VIC, Australia

³Australian Research Council Centre of Excellence for the Weather of the 21st Century, Australia

(Received xx; revised xx; accepted xx)

This paper explores decaying turbulence beneath surface waves that is initially isotropic and shear-free. We start by presenting phenomenology revealed by wave-averaged numerical simulations: an accumulation of angular momentum in coherent vortices perpendicular to the direction of wave propagation, suppression of kinetic energy dissipation, and the development of depth-alternating jets. We interpret these features through an analogy with rotating turbulence (Holm 1996), wherein the curl of the Stokes drift, $\nabla \times \mathbf{u}^S$, takes on the role of the background vorticity (for example, $(f_0 + \beta y)\hat{z}$ on the beta plane). We pursue this thread further by showing that a two-equation model proposed by Bardina *et al.* (1985) for rotating turbulence reproduces the simulated evolution of volume-integrated kinetic energy. This success of the two-equation model — which explicitly parametrizes wave-driven suppression of kinetic energy dissipation — carries implications for modeling turbulent mixing in the ocean surface boundary layer. We conclude with a discussion about a wave-averaged analogue of the Rossby number appearing in the two-equation model, which we term the “pseudovorticity number” after the pseudovorticity $\nabla \times \mathbf{u}^S$. The pseudovorticity number is related to the Langmuir number in an integral sense.

1. Introduction

Surface waves modulate near-surface ocean turbulent mixing, especially in summertime and in the tropics where boundary layers are often shallow, sunny, windy, and wavy (Sullivan & McWilliams 2010). Turbulence driven by surface wind stress and affected by surface waves is usually called “Langmuir turbulence” (McWilliams *et al.* 1997), implying a connection between wave-catalyzed turbulent coherent structures and the structure of a laminar, wave-catalyzed shear instability that Craik & Leibovich (1976) called “Langmuir circulation”.

In this paper we investigate decaying turbulence beneath surface waves using numerical simulations of the wave-averaged Navier–Stokes equations (Craik & Leibovich 1976). Decaying turbulence is fundamental (Batchelor 1953) but has seen little attention beneath surface waves. Most work on wave-modified turbulence involves strong ambient shear and also invokes surface forcing by winds and buoyancy fluxes (McWilliams *et al.* 1997; Polton *et al.* 2005; Harcourt & D’Asaro 2008; Van Roekel *et al.* 2012; Large *et al.* 2019; Fan *et al.*

† Email address for correspondence: wagner.greg@gmail.com

2020). We show that some of the essential phenomenology of turbulence beneath surface waves is revealed by focusing on the evolution of unforced, initially-shear-free turbulence.

We interpret the results of these simulations in section 2, leveraging an analogy between wave-averaged and rotating dynamics first proposed by Holm (1996). Like rotation, surface waves *catalyze* a transfer of energy from smaller to larger scales (hereby referred to as ‘inverse cascade’) within the turbulent flow beneath the waves — without exchanging energy with the flow — and cause angular momentum to accumulate in coherent vortices, while suppressing kinetic energy dissipation. This contrasts our case with the interaction between balanced flows and internal waves, wherein non-catalytic interactions can occur even for steady wave fields (Thomas 2023). Moreover, unlike in shear-driven Langmuir turbulence where coherent structures tend to align with the direction of the Lagrangian-mean shear (Sullivan & McWilliams 2010; Van Roekel *et al.* 2012), the coherent vortices that we observe forming in the absence of shear are instead oriented *perpendicular to the direction of surface wave propagation*. We also observe the development of alternating jets, as in beta-plane turbulence.

In section 3 we further the analogy by adapting a phenomenological model proposed by Bardina *et al.* (1985) for decaying rotating turbulence to the wave-averaged case, showing that the model also describes the decay of volume-averaged kinetic energy beneath surface waves. This model suggests a new way to incorporate wave effects into two-equation models (for example, Harcourt (2015)) by explicitly representing the surface-wave-driven suppression of kinetic energy dissipation.

We conclude in section 4 by proposing a new non-dimensional number to characterize the importance of surface waves for the evolution of turbulent flows analogous to the Rossby number. We show how this new number may be related to the Langmuir number for wind-forced cases, while also generalizing to purely convective or decaying situations.

2. Simulations of decaying turbulence beneath surface waves

The incompressible, inviscid momentum equation in the presence of a background vorticity Ω ,

$$\partial_t \mathbf{u} + (\mathbf{u} \cdot \nabla) \mathbf{u} + \Omega \times \mathbf{u} + \nabla p = 0, \quad \text{with} \quad \nabla \cdot \mathbf{u} = 0, \quad (2.1)$$

describes *both* rotating flows without surface waves and *also* wave-averaged flows beneath steady, horizontally-uniform surface-wave fields (see for example Craik & Leibovich 1976; Suzuki & Fox-Kemper 2016; Holm 1996; Wagner *et al.* 2021). In the wave-averaged case, p and \mathbf{u} in (2.1) represent the Eulerian-mean kinematic pressure and Lagrangian-mean velocity, respectively. The Lagrangian-mean velocity is the “total” velocity responsible for the advection of mass, momentum, tracers, and particles, and may be decomposed into an Eulerian-mean component plus “Stokes drift” correction (van den Bremer & Breivik 2018; Vanneste & Young 2022, see for example). The wave-averaged momentum equation may be derived by asymptotic expansion leveraging a time-scale separation between rapidly oscillating surface waves and the slower evolution of \mathbf{u} (Craik & Leibovich 1976; Leibovich 1980; Vanneste & Young 2022). The appearance of surface waves in (2.1) as an effective Coriolis force is discussed by Holm (1996).

For rotating flows, the background vorticity Ω in (2.1) takes the form

$$\Omega_{\text{rotating}} = f \hat{z}, \quad (2.2)$$

where f is the Coriolis parameter and \hat{z} is the axis of rotation. For wave-averaged flows beneath a uniform surface wave field propagating in the x direction, the background

vorticity $\boldsymbol{\Omega}$ is alternatively

$$\boldsymbol{\Omega}_{\text{waves}} = -\nabla \times \mathbf{u}^S = -\partial_z u^S \hat{\mathbf{y}}, \quad (2.3)$$

where $\mathbf{u}^S = u^S(z)\hat{\mathbf{x}}$ is the surface wave Stokes drift (Craik & Leibovich 1976; Suzuki & Fox-Kemper 2016; van den Bremer & Breivik 2018; Vanneste & Young 2022). We refer to $\nabla \times \mathbf{u}^S$ — the curl of Stokes drift and therefore the curl of pseudomomentum Andrews & McIntyre (1978) — as the “pseudovorticity”. (Stokes drift and pseudomomentum are identical for surface waves (McIntyre 1981). Conceptually and more generally, “Stokes drift” is the difference between the Eulerian-mean and Lagrangian-mean momentum, while “pseudomomentum” is an apparent, wave-affiliated momentum that appears in the mean momentum budget.) In the context of equation (2.1), the main difference between rotating turbulence and turbulence beneath steady surface waves is the spatial structure of $\partial_z u^S$: in shallow water $\partial_z u^S \sim z$ to leading-order, while $\partial_z u^S$ decays exponentially for deep water waves.

2.1. Coherent structures in rotating and wave-averaged turbulence

To illustrate the similarity of rotating turbulence and turbulence beneath surface waves we conduct large eddy simulations of equation (2.1) with implicit grid-scale dissipation in a unit cube with three choices for $\boldsymbol{\Omega}$,

$$\boldsymbol{\Omega}_{\text{rotating}} = \frac{1}{4}\hat{\mathbf{z}}, \quad \boldsymbol{\Omega}_{\text{waves}} = -\frac{1}{2}z\hat{\mathbf{y}}, \quad \text{and} \quad \boldsymbol{\Omega}_{\text{isotropic}} = 0. \quad (2.4)$$

Above, $\frac{1}{2}z$ is the pseudovorticity associated with a shallow water wave in $z \in [0, 1]$ with Stokes drift $\mathbf{u}^S \approx \frac{1}{2}(1 + \frac{1}{2}z^2)\hat{\mathbf{x}}$. Note that turbulence beneath shallow water waves is homeomorphic to β -plane turbulence Rhines (1975) — with $\boldsymbol{\Omega}_{\beta\text{-plane}} = \beta y\hat{\mathbf{z}}$ — modulo on the xz plane instead of on the xy plane and with the Stokes drift curvature $\partial_z^2 u^S$ playing the role of β .

The simulation domain is horizontally-periodic in x, y , and we use free-slip boundary conditions at the top and bottom boundaries in z . Implicit dissipation of grid-scale kinetic energy is provided by an upwind-biased, nominally 9th-order Weighted, Essentially Non-Oscillatory advection scheme (Pressel *et al.* 2017; Shu 2020; Silvestri *et al.* 2024). Our implicit dissipation method allows us to simulate decaying turbulence that undergoes a transition from isotropic to nearly two-dimensional dynamics.

Following previous isotropic homogeneous turbulence studies (e.g., Orszag & Patterson (1972)), we produce an initial condition for the three simulations by conducting a preliminary simulation initialized with kinetic energy spectrum

$$\frac{1}{2}|\hat{\mathbf{u}}|^2 \sim |\mathbf{K}|^2 \exp \left\{ -2 \left(|\mathbf{K}| / K_i \right)^2 \right\}, \quad (2.5)$$

where $\hat{\mathbf{u}}$ is the Fourier transform of \mathbf{u} , \mathbf{K} is the Fourier wavenumber vector, and $K_i = 32 \times 2\pi$ is the 32nd wavenumber in the domain. The amplitude of the preliminary initial condition is scaled to produce an initial root-mean-square vorticity

$$\sqrt{\int |\omega|^2 dV} \stackrel{\text{def}}{=} \omega_{\text{rms}}(t = -t_0) = 1000, \quad \text{where} \quad \omega \stackrel{\text{def}}{=} \nabla \times \mathbf{u} = \xi \hat{\mathbf{x}} + \eta \hat{\mathbf{y}} + \zeta \hat{\mathbf{z}}. \quad (2.6)$$

The initial simulation is run for a duration t_0 until $t = 0$, defined as the time when the mean-square vorticity has decayed to $\omega_{\text{rms}}(t = 0) = 10$. The velocity field is then saved to disk to be used as an initial condition in subsequent runs starting from $t = 0$. The simulations are conducted with Oceananigans (Ramadhan *et al.* 2020; Wagner *et al.* 2025), which discretizes (2.1) with a finite volume method. Scripts that reproduce simulations in this paper are stored on GitHub; see the Data availability statement.

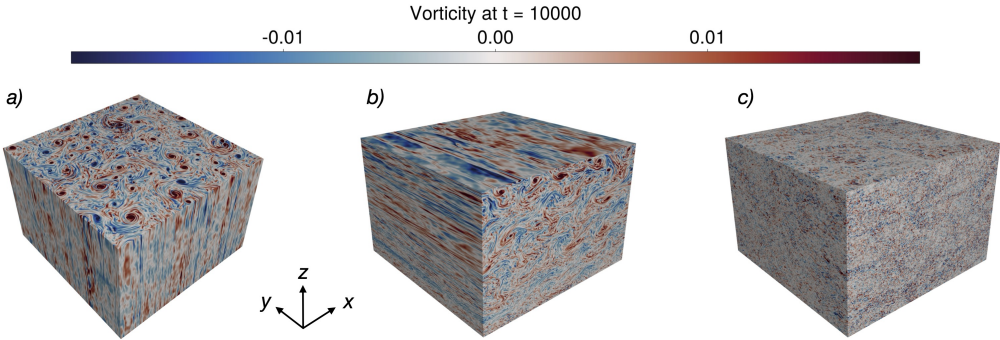


Figure 1: Vorticity in simulations decaying turbulence with 512^3 finite volume cells in a unit cube after 1000 time units. (a) Vertical relative vorticity $\zeta = \hat{z} \cdot (\nabla \times \mathbf{u})$ in rotating turbulence with Coriolis parameter $f = 1/4$, (b) Horizontal relative vorticity $\eta = \hat{j} \cdot (\nabla \times \mathbf{u})$ in turbulence beneath surface waves with Stokes shear $\partial_z u^S = -z/2$, and (c) η in isotropic turbulence.

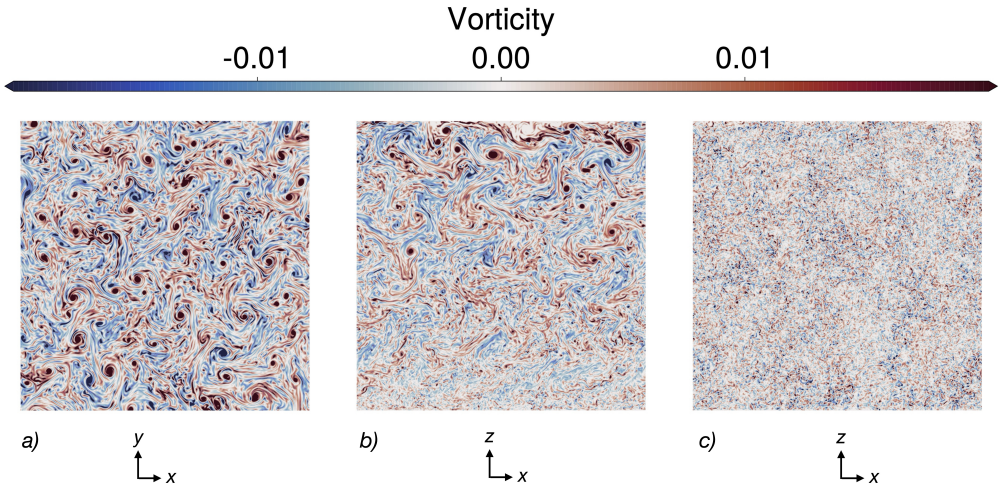


Figure 2: As figure 1 but showing (a) ζ for rotating turbulence in the xy -plane; (b) η for turbulence beneath surface waves in the xz -plane, (c) η for isotropic turbulence in the xz -plane.

We focus first on the evolution of the relative vorticity ω defined in equation (2.6). Figure 1 shows vorticity components for the three cases after $t = 1000$ time units: figure 1(a) shows vertical vorticity ζ , while figures 1(b) and (c) show the horizontal vorticity η . Figure 1(a) and (b) for rotating and wave-affected turbulence, respectively, both exhibit the formation of coherent structures and relatively greater vorticity levels than the unorganized, small amplitude isotropic vorticity in figure 1(c). Figure 2 is similar, except that figure 2(a) shows ζ in rotating turbulence in the xy -plane, while figures 2(b) and 2(c) show η in the xz plane for wave-averaged and isotropic turbulence, respectively.

2.2. Zonation and the analogy of wave-averaged turbulence with beta-plane turbulence

One of the most striking aspects of the similarity between β -plane turbulence and turbulence beneath surface waves is the development of “zonal jets” — coherent, alternating jets in the

direction of surface wave propagation (and perpendicular to the pseudovorticity direction). This similarity allows us, therefore, to borrow intuition on structure formation in β -plane turbulence (for example, Huang & Robinson (1998); Farrell & Ioannou (2007); Srinivasan & Young (2012); Constantinou *et al.* (2014); for an overview see Constantinou (2015); Farrell & Ioannou (2019); Marston & Tobias (2023).)

To illustrate this, we consider two additional cases with background vorticity

$$\boldsymbol{\Omega}_{\text{deep}} = -\frac{1}{4}e^{8(z-1)}\hat{\mathbf{y}}. \quad \text{and} \quad \boldsymbol{\Omega}_{\text{weak}} = -\frac{1}{8}z\hat{\mathbf{y}}. \quad (2.7)$$

These and subsequent simulations use 384^3 finite volume cells to reduce their computational expense for the purpose of performing longer simulations to $t = 10^4$.

Figure 3 shows time-series of the y -momentum v , which plays the role that vertical velocity plays in rotating turbulence. The right side of figure 3 shows vertical profiles of the horizontally-averaged x -momentum,

$$U(z, t) \stackrel{\text{def}}{=} \int u \, dx \, dy. \quad (2.8)$$

These U -profiles exhibit the development of depth-alternating jets, which are most prominently exhibited by the zig-zagging structure in the medium waves case on the right side of figure 3. To our knowledge, depth-alternating jets have not been observed in shear-free wave-modified turbulence. Comparing the slices of v for medium and weak waves reveals how the medium-strong waves induce a strong inverse cascade, more coherent vortices, and fewer small-scale motions than the weak waves.

3. Phenomenological model for the evolution of kinetic energy

We turn to the evolution of the domain-averaged kinetic energy,

$$k(t) \stackrel{\text{def}}{=} \int \frac{1}{2} (u^2 + v^2 + w^2) \, dV. \quad (3.1)$$

Figure 4 plots time-series of the normalized kinetic energy $k(t)/k(t = 0)$ for the three cases presented in figure 1, as well as three additional cases that use $\boldsymbol{\Omega} = Sz\hat{\mathbf{y}}$ with $S = (1/2, 1/8, 1/16)$. Figure 4 illustrates another common feature to rotating turbulence and turbulence beneath surface waves: a suppression of the kinetic energy dissipation rate, such that at long times the kinetic energy levels off. We theorize that the suppression of dissipation is linked to the formation of coherent structures: rather than cascading to the grid scale, where dissipation can occur, kinetic energy accumulates in much larger-scale coherent structures. Similar to the dynamics of two-dimensional turbulence McWilliams (1984), the concentration of kinetic energy in coherent structures suppresses the forward cascade of kinetic energy.

Inspired by Bardina *et al.* (1985), we model the kinetic energy $k(t)$ with the phenomenological two-equation system

$$\frac{d}{dt} k = -\epsilon, \quad (3.2)$$

$$\frac{d}{dt} \epsilon = -a \frac{\epsilon^2}{k} - b\Omega\epsilon, \quad (3.3)$$

where $\epsilon(t)$ describes the dissipation rate of k , Ω is a characteristic scale for $\boldsymbol{\Omega}$, and a and b are $O(1)$ free parameters. Equation (3.2) follows directly from $\int \mathbf{u} \cdot (\mathbf{2.1}) \, dV$ after accounting for the effect of the implicit numerical dissipation in our simulations. (Alternative models

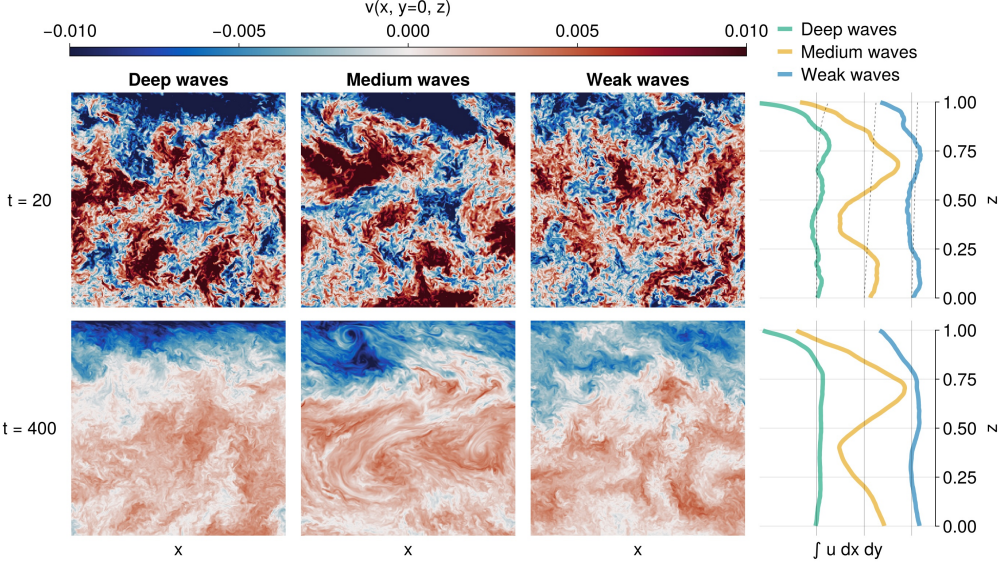


Figure 3: The evolution of cross-wave momentum v in the xz -plane (6 panels on the left) and horizontally-averaged along-wave-momentum u (2 panels on the right) at $t = 40, 400$ and for three wave fields: “deep” (left panel, red lines), “medium” (middle panel, orange lines), and “weak” (right panel, blue lines). Dashed lines in the top right plot show the Stokes drift profile (normalized) for each case. The “medium” waves case uses the background vorticity Ω_{waves} in (2.4). Both the u profiles and the light gray “zero lines” are spaced apart by the scale $\delta u = 10^{-2}$. The u -profiles at right show the development of depth-alternating jets, including a counter-wave surface jet for all cases. The v -slices are similar between the three cases at early times, but at later times exhibit strong, localized wave-impacts in their respective regions of significant Stokes shear. Note that v plays the role that vertical velocity plays in rotating turbulence. Note that the Rhines scale may be estimated as $\ell_R = 2\pi\sqrt{U/|\partial_z^2 u^S|}$. With $|\partial_z^2 u^S| = \frac{1}{2}$ and $U \approx 10^{-2}$ for the medium waves case, for example, we estimate $\ell_R \approx 0.8$, consistent with the jet spacing apparent on the right panels.

that include surface-wave-associated source terms for turbulent kinetic energy, such as the one proposed by Axell (2002), are inconsistent with (2.1).) The catalytic nature of rotation or surface waves may also be deduced from the fact that Ω does not appear in equation (3.2). The first term in (3.3) models the destruction of ϵ on the turbulent time-scale $\tau = k/\epsilon$, since $d\epsilon/dt \sim -\epsilon/\tau$ when $\Omega\epsilon \ll \epsilon/\tau$.

The second term in (3.3) models the suppression of kinetic energy dissipation — or alternatively, the growth of the correlation length due to the coalescence of coherent structures — by the background vorticity Ω . The relative importance of “intrinsic” destruction of ϵ and background-vorticity-induced destruction of ϵ is measured by the non-dimensional number $\Omega\tau = \Omega k/\epsilon$, whose significance is revisited in section 4. We note that (3.2) is exact — and unchanged whether or not the system is rotating or modulated by surface waves. The modulation of turbulence by surface waves is therefore fundamentally “catalytic”, and can only affect k indirectly by changing (3.3).

The free parameter a may be constrained by considering isotropic turbulence with $\Omega = 0$. In this case we expect the turbulent kinetic energy to decay according to $k \sim t^{-6/5}$ (Saffman

1967), which implies $\frac{d}{dt}k = -\frac{6}{5}\frac{k}{t}$, and thus in turn, via (3.2), leads to

$$\epsilon = \frac{6}{5}\frac{k}{t}, \quad \text{so that} \quad \frac{d}{dt}\epsilon = -\frac{66}{25}\frac{k}{t^2}. \quad (3.4)$$

Inserting (3.4) into (3.3) yields $a = 11/6$.

From (3.2)–(3.3) we deduce that the rate of change of the combination $\log \epsilon - a \log k$ is proportional to b , that is,

$$\frac{d}{dt}(\log \epsilon - a \log k) = -b\Omega. \quad (3.5)$$

Integrating (3.5) produces

$$\frac{\epsilon}{\epsilon_0} = \left(\frac{k}{k_0}\right)^a e^{-b\Omega t}, \quad (3.6)$$

where ϵ_0 and k_0 are the dissipation and kinetic energy at $t = 0$ respectively. If we insert the expression for the dissipation $\epsilon(t)$ from (3.6) into (3.2) and integrate in time, we obtain

$$\frac{k}{k_0} = \left[1 + \frac{1}{nb\Omega} \frac{\epsilon_0}{k_0} \left(1 - e^{-b\Omega t}\right)\right]^{-n}, \quad (3.7)$$

where $n = 1/(a - 1) = 6/5$. (See also equation (10) in Bardina *et al.* (1985).) Taking the limit $\Omega \rightarrow 0$ (or $t \rightarrow 0$ with finite Ω), we obtain the corresponding solution for isotropic turbulence,

$$k_{\text{isotropic}}(t) = k_0 \left(1 + \frac{1}{n} \frac{\epsilon_0}{k_0} t\right)^{-n}, \quad (3.8)$$

which yields the expected power law $k \sim t^{-n}$ when $\epsilon_0 t / nk_0 \gg 1$.

At long times the isotropic and vortical solutions diverge: $k_{\text{isotropic}} \rightarrow 0$ as $t \rightarrow \infty$, while in the vortical case k/k_∞ limits to the constant

$$\frac{k_\infty}{k_0} = \left(1 + \frac{\epsilon_0}{nb\Omega k_0}\right)^{-n}, \quad (3.9)$$

where $k_\infty = \lim_{t \rightarrow \infty} k(t)$. Equation (3.9) yields a formula for b in terms of k_∞ ,

$$b\Omega = \frac{\epsilon_0}{nk_0} \frac{1}{\left(\frac{k_\infty}{k_0}\right)^{1/n} - 1}, \quad (3.10)$$

which we use to diagnose b from our numerical simulations.

The dashed curves in figure 4 show solutions to the two-equation system in (3.2)–(3.3) that correspond to the solid-line simulated results. Figure 4 shows that a single value of $b = 0.036$ qualitatively describes the evolution of kinetic energy beneath surface waves for a wide range of background vorticity magnitudes Ω , where we estimate Ω via the z -average of $\partial_z u^S$, that is $\Omega \approx \int \partial_z u^S dz$. For the rotating case, we use $b = 0.033$ and $\Omega = 1/4$. While qualitatively excellent considering that $b \approx 0.036$ describes a wide range of conditions, we also find that the phenomenological model overestimates the dissipation rate — and therefore underestimates the kinetic energy k — during the transition between isotropic and background-vorticity-dominated regimes.

4. Discussion

In this paper we point out the similarity between rotating turbulence on the beta-plane and turbulence beneath surface waves. In particular, turbulence beneath surface waves exhibits

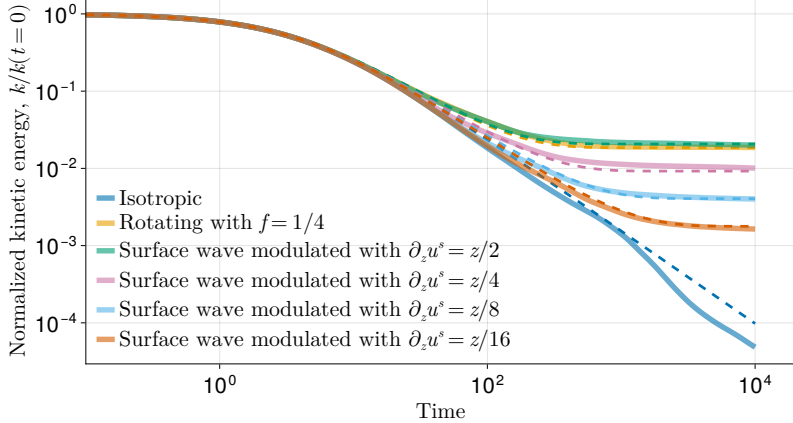


Figure 4: The decay of kinetic energy $k(t)$ in isotropic, rotating, and surface-wave-modulated turbulence. Solid lines show kinetic energy normalized by its initial value, k/k_0 , computed from large eddy simulations. Dashed lines show k/k_0 given by (3.7), which solves the phenomenological two-equation system in (3.2)–(3.3). The initial dissipation rate ϵ_0 in (3.7) is estimated from the numerical solution; specifically we evaluate (3.8) at Δt , substitute $k(t = \Delta t)$ from the numerical solution, and solve for ϵ_0 . We use $a = 11/6$ and estimate b from (3.10). For the rotating case, $\Omega = 1/4$ yields $b = 0.033$.

For the four surface-wave-modulated cases we use $b = 0.036$, where

$$\Omega \stackrel{\text{def}}{=} \int \partial_z u^S dz = (1/4, 1/8, 1/16, 1/32). \text{ Note that using } a = 1.75 \text{ along with commensurate adjustments to } b \text{ matches the simulation data even more closely.}$$

the formation of coherent structures perpendicular to the direction of wave propagation, the development of zonal jets, and the suppression of kinetic energy dissipation. These features are consistent with known properties of turbulence beneath surface waves, but the connection with rotating turbulence is obscured in studies that also involve surface wind stress, ambient Lagrangian-mean shear, and surface forcing. In particular, we hypothesize that some of the generic features of Langmuir turbulence — such as the formation of coherent structures, a suppression of kinetic energy dissipation, and an increase in mixing — are driven by similar dynamics as the phenomenon observed in our decaying situations. At the same time, however, the presence of Lagrangian-mean shear produces additional and distinctly different phenomenon, most clearly in the alignment of coherent vortices with the Lagrangian-mean shear, rather than perpendicular to the direction of wave propagation.

We exploit the connection to rotating turbulence by adapting a phenomenological two-equation model proposed by Bardina *et al.* (1985). In this two-equation model, the evolution of dissipation is affected by two terms: one “classical” term producing power-law decay of kinetic energy, and a second term that describes the suppression of kinetic energy dissipation by the presence of surface waves, which in turn effectively enhances kinetic energy levels and turbulent mixing relative to pure isotropic turbulence.

This phenomenological model hints at a new way to understand how surface waves modulate turbulent mixing. In the paradigm proposed by McWilliams *et al.* (1997), the effect of surface waves on turbulence is associated with the “Stokes contribution” to shear production in the turbulent kinetic energy budget. However, our results show that this interpretation must be incomplete, because surface waves also control the evolution of initially shear-free flows.

We therefore propose an alternative theory which supposes that the impact of surface waves may be instead linked to their tendency to catalyze, without exchanging energy, an increase

in the correlation times and length scales of turbulent motions. A benefit to our alternative interpretation is that turbulent shear production can be interpreted in the standard way: as a transfer of kinetic energy from the horizontally-averaged, Lagrangian-mean velocity, whose energy is otherwise conserved. In other words, our descriptive analysis leads to an alternative paradigm for wave-modified turbulence wherein shear production is “unchanged” relative to wave-free turbulence (as in rotating turbulence). Instead of modifying shear production directly, then, waves impact both mixing and kinetic energy by inducing an inverse cascade, increasing the turbulent mixing length, and suppressing kinetic energy dissipation.

4.1. The “pseudovorticity” number

The analogy with rotating turbulence inspires the definition of a new non-dimensional number for characterizing surface wave effects on turbulence. In rotating turbulence, the Rossby number measures the relative magnitude of the relative vorticity $\nabla \times \mathbf{u}$ and the background vorticity, $f\hat{\mathbf{z}}$, such that

$$\text{Ro} \stackrel{\text{def}}{=} \frac{|\nabla \times \mathbf{u}|}{f} \sim \frac{U}{fL}, \quad (4.1)$$

where U is a characteristic horizontal velocity scale and L is a characteristic turbulent horizontal scale. We propose the analogous “pseudovorticity number” for boundary layer turbulence,

$$\text{Ps} \stackrel{\text{def}}{=} \frac{|\nabla \times \mathbf{u}|}{|\partial_z \mathbf{u}^S|} \sim \frac{W}{\Omega H}, \quad (4.2)$$

where W is a turbulence velocity scale, Ω is the magnitude of the Stokes drift shear, and H is a turbulence length scale. In boundary layer turbulence, for example, W and H are most straightforwardly measured by the magnitude of the vertical velocity and the boundary layer depth.

The pseudovorticity number Ps measures the average role of surface waves with Stokes shear magnitude Ω on turbulent motions with turbulent velocity scale W and turbulent length scale H . In the two-equation model in (3.2)–(3.3), $\text{Ps} \sim \epsilon/k\Omega$. In our decaying scenarios, Ps eventually vanishes at $t \rightarrow \infty$ and dissipation is completely suppressed.

4.2. Connection with the Langmuir number

The pseudovorticity number is connected between the Langmuir number — the usual non-dimensional quantity used to characterize the effect of waves on turbulence — when considering an estimate of Ps integrated over deep boundary layers. One definition of the Langmuir number is (McWilliams *et al.* 1997),

$$\text{La} \stackrel{\text{def}}{=} \sqrt{\frac{u_\star}{u^S(z=0)}}, \quad (4.3)$$

where u_\star is the friction velocity, which is the square root of the kinematic wind stress. At face value, La does not apply to decaying cases, but we can amend this by interpreting u_\star more generally as a turbulent velocity scale.

To connect La and Ps , we consider a “bulk” estimate of Ps over a wind-forced boundary layer of depth H , where the turbulent velocity scale is $W = u_\star$ and the turbulent length scale is H . If $u^S(z = -H)$ is negligible, then estimating the pseudovorticity scale Ω as the average value over the boundary layer yields

$$\Omega \sim \frac{1}{H} \int_{-H}^0 \partial_z u^S dz \sim \frac{u^S(z=0)}{H}, \quad (4.4)$$

such that

$$\text{bulk Ps} = \frac{W}{\Omega H} \sim \frac{u_\star}{u^S(z=0)} \sim La^2. \quad (4.5)$$

We thus find that La^2 may be regarded as a bulk estimate of the more locally-applicable Ps , computed over the depth of the boundary layer, H . The difference between the bulk estimate La and the more specific estimate Ps resolves a paradox associated with La in that it depends on u^S , despite that only $\partial_z u^S$ appears in (2.1).

Acknowledgements. Without implying their endorsement, we would like to acknowledge fruitful discussions with Bruno Deremble, Petros Ioannou, and Bill Young. We would also like to thank the editor and the three anonymous reviewers for their constructive comments that greatly improved our paper. Part of this work was done during the Sean R. Haney Memorial Symposium 2025 at the Scripps Institution of Oceanography in La Jolla, California.

Funding. G.L.W. was supported by the National Science Foundation, grant OCE-2342715. N.C.C. was supported by the Australian Research Council under the DECRA Fellowship DE210100749, the Center of Excellence for the Weather of the 21st Century CE230100012, and the Discovery Project DP240101274.

Declaration of interests. The authors report no conflict of interest.

Data availability statement. Scripts to reproduce the simulations and analyses in this of this study are openly available at the GitHub repository github.com/glwagner/WaveAveragedDecayingTurbulence.

Simulation output used to produced the figures in this paper will be uploaded in a Zenodo repository upon acceptance.

Author ORCIDs. Gregory L. Wagner, [0000-0001-5317-2445](https://orcid.org/0000-0001-5317-2445); Navid C. Constantinou, [0000-0002-8149-4094](https://orcid.org/0000-0002-8149-4094).

REFERENCES

- ANDREWS, D. G. & MCINTYRE, M. E. 1978 An exact theory of nonlinear waves on a Lagrangian-mean flow. *J. Fluid Mech.* **89** (4), 609–646.
- AXELL, L. B. 2002 Wind-driven internal waves and Langmuir circulations in a numerical ocean model of the southern Baltic Sea. *J. Geophys. Res. Oceans* **107** (C11), 25–1.
- BARDINA, J., FERZIGER, J. H. & ROGALLO, R. S. 1985 Effect of rotation on isotropic turbulence: computation and modelling. *J. Fluid Mech.* **154**, 321–336.
- BATCHELOR, G. K. 1953 *The theory of homogeneous turbulence*. Cambridge University Press.
- VAN DEN BREMER, T. S. & BREIVIK, Ø. 2018 Stokes drift. *Philos. T. R. Soc. A* **376** (2111), 20170104.
- CONSTANTINOU, N. C. 2015 Formation of large-scale structures by turbulence in rotating planets. PhD thesis, National and Kapodistrian University of Athens, Athens, Greece.
- CONSTANTINOU, N. C., FARRELL, B. F. & IOANNOU, P. J. 2014 Emergence and equilibration of jets in beta-plane turbulence: Applications of Stochastic Structural Stability Theory. *J. Atmos. Sci.* **71** (5), 1818–1842.
- CRAIK, A. D. D. & LEIBOVICH, S. 1976 A rational model for Langmuir circulations. *J. Fluid Mech.* **73** (3), 401–426.
- FAN, Y., YU, Z., SAVELYEV, I., SULLIVAN, P. P., LIANG, J.-H., HAACK, T., TERRILL, E., DE PAOLO, T. & SHEARMAN, K. 2020 The effect of Langmuir turbulence under complex real oceanic and meteorological forcing. *Ocean Model.* **149**, 101601.
- FARRELL, B. F. & IOANNOU, P. J. 2007 Structure and spacing of jets in barotropic turbulence. *J. Atmos. Sci.* **64** (10), 3652–3665.
- FARRELL, B. F. & IOANNOU, P. J. 2019 Statistical State Dynamics: A new perspective on turbulence in shear flow. In *Zonal jets: Phenomenology, genesis, and physics* (ed. B. Galperin & P. L. Read), p. 380–400. Cambridge University Press.
- HARCOURT, R. R. 2015 An improved second-moment closure model of Langmuir turbulence. *J. Phys. Oceanogr.* **45** (1), 84–103.
- HARCOURT, R. R. & D'ASARO, E. A. 2008 Large-eddy simulation of Langmuir turbulence in pure wind seas. *J. Phys. Oceanogr.* **38** (7), 1542–1562.
- HOLM, D. D. 1996 The ideal Craik–Leibovich equations. *Physica D* **98** (2–4), 415–441.

- HUANG, H.-P. & ROBINSON, W. A. 1998 Two-dimensional turbulence and persistent zonal jets in a global barotropic model. *J. Atmos. Sci.* **55** (4), 611–632.
- LARGE, W. G., PATTON, E. G., DUVIVIER, A. K., SULLIVAN, P. P. & ROMERO, L. 2019 Similarity theory in the surface layer of large-eddy simulations of the wind-, wave-, and buoyancy-forced southern ocean. *J. Phys. Oceanogr.* **49** (8), 2165–2187.
- LEIBOVICH, S. 1980 On wave-current interaction theories of langmuir circulations. *J. Fluid Mech.* **99** (4), 715–724.
- MARSTON, J. B. & TOBIAS, S. M. 2023 Recent developments in theories of inhomogeneous and anisotropic turbulence. *Annu. Rev. Fluid Mech.* **55**, 351–375.
- MCINTYRE, ME 1981 On the ‘wave momentum’ myth. *Journal of Fluid Mechanics* **106**, 331–347.
- MCKWILLIAMS, J. C. 1984 The emergence of isolated coherent vortices in turbulent flow. *J. Fluid Mech.* **146**, 21–43.
- MCKWILLIAMS, J. C., SULLIVAN, P. P. & MOENG, C.-H. 1997 Langmuir turbulence in the ocean. *J. Fluid Mech.* **334**, 1–30.
- ORSZAG, S. A. & PATTERSON, G. S. 1972 Numerical simulation of three-dimensional homogeneous isotropic turbulence. *Phys. Rev. Lett.* **28**, 76–79.
- POLTON, J. A., LEWIS, D. M. & BELCHER, S. E. 2005 The role of wave-induced Coriolis–Stokes forcing on the wind-driven mixed layer. *J. Phys. Oceanogr.* **35** (4), 444–457.
- PRESSEL, K. G., MISHRA, S., SCHNEIDER, T., KAUL, C. M. & TAN, Z. 2017 Numerics and subgrid-scale modeling in large eddy simulations of stratocumulus clouds. *J. Adv. Model. Earth Syst.* **9** (2), 1342–1365.
- RAMADHAN, A., WAGNER, G. L., HILL, C., CAMPIN, J.-M., CHURAVY, V., BESARD, T., SOUZA, A., EDELMAN, A., FERRARI, R. & MARSHALL, J. 2020 Oceananigans.jl: Fast and friendly geophysical fluid dynamics on GPUs. *J. Open Source Softw.* **5** (53), 2018.
- RHINES, P. B. 1975 Waves and turbulence on a beta-plane. *J. Fluid Mech.* **69** (3), 417–443.
- SAFFMAN, P. G. 1967 The large-scale structure of homogeneous turbulence. *J. Fluid Mech.* **27** (3), 581–593.
- SHU, C.-W. 2020 Essentially non-oscillatory and weighted essentially non-oscillatory schemes. *Acta Numer.* **29**, 701–762.
- SILVESTRI, S., WAGNER, G. L., CAMPIN, J.-M., CONSTANTINOU, N. C., HILL, C. N., SOUZA, A. & FERRARI, R. 2024 A new WENO-based momentum advection scheme for simulations of ocean mesoscale turbulence. *J. Adv. Model. Earth Syst.* **16** (7), e2023MS004130.
- SRINIVASAN, K. & YOUNG, W. R. 2012 Zonostrophic instability. *J. Atmos. Sci.* **69** (5), 1633–1656.
- SULLIVAN, P. P. & MCKWILLIAMS, J. C. 2010 Dynamics of winds and currents coupled to surface waves. *Annu. Rev. Fluid Mech.* **42** (1), 19–42.
- SUZUKI, N. & FOX-KEMPER, B. 2016 Understanding Stokes forces in the wave-averaged equations. *J. Geophys. Res. Oceans* **121** (5), 3579–3596.
- THOMAS, J. 2023 Turbulent wave-balance exchanges in the ocean. *Proc. R. Soc. A* **479** (2276), 20220565.
- VAN ROEKEL, L. P., FOX-KEMPER, B., SULLIVAN, P. P., HAMILTON, P. E. & HANEY, S. R. 2012 The form and orientation of Langmuir cells for misaligned winds and waves. *J. Geophys. Res. Oceans* **117** (C5).
- VANNESTE, J. & YOUNG, W. R. 2022 Stokes drift and its discontents. *Philos. T. R. Soc. A* **380** (2225), 20210032.
- WAGNER, G. L., CHINI, G. P., RAMADHAN, A., GALLET, B. & FERRARI, R. 2021 Near-inertial waves and turbulence driven by the growth of swell. *J. Phys. Oceanogr.* **51** (5), 1337–1351.
- WAGNER, G. L., SILVESTRI, S., CONSTANTINOU, N. C., RAMADHAN, A., CAMPIN, J.-M., HILL, C., CHOR, T., STRONG-WRIGHT, J., LEE, X. K., POULIN, F., SOUZA, A., BURNS, K. J., MARSHALL, J. & FERRARI, R. 2025 High-level, high-resolution ocean modeling at all scales with Oceananigans. *arXiv preprint*, arXiv: 2502.14148.